RAL-TR-2001-024

THE OPERATION OF GAS MICROSTRIP DETECTORS IN ELECTRONEGATIVE GAS MIXTURES

J.E. Bateman

Rutherford Appleton Laboratory, Chilton, Didcot, Oxon, OX11 0QX, U.K.

10 May 2001

Abstract

As with all gas counters, the performance of gas microstrip detectors (GMSD) can be seriously compromised by the presence of electronegative gas components (or pollutants). In contrast to conventional proportional counters, the geometry of the GMSD permits the drift electric field to be controlled independently of the avalanche gain field. This permits the monitoring and minimisation of the effects of electronegative gas components. Simple mathematical models are derived which allow quantitation of the electron attachment length from its effect on the pulse height distributions obtained from x-ray line spectra. The effects of electron attachment on x-ray energy resolution, linearity and also on auger electron spectra are discussed.

1. Introduction

Gas avalanche counters in general and Gas Microstrip Detectors (GMSD) [1] in particular, have the unrivalled capability of providing a wide range of active detecting media by the simple expedient of changing the operating gas mixture. Thus charged particles, x-rays and neutrons can be detected over a wide range of energies. The current availability of low noise electronic amplifiers enables gas mixtures with relatively poor gain characteristics (i.e. a maximum avalanche gain of a few hundred) to be utilised as demanded by the application. However, the low density of the gas medium generally demands that active volumes of depth of a few centimetres are used. For the avalanche process to occur, the thermal electrons released in the gas by the incident radiation must be transported to the detector anodes (typically wires or narrow strips of metallization) where they generate an avalanche process in the high electric fields present. With the exception of hydrogen and the noble gases all gas molecules have a finite cross-section for the capture of a free electron and its conversion into a negative ion. Any electron so captured is lost to the avalanche process and causes a proportionate loss in the detected pulse. This process is known as *electron attachment*, and is one of the chief limitations on the molecular gases which may be successfully used inside a gas counter.

The electron attachment properties of a gas mixture can be characterised by a single parameter known as the *attachment length* (λ). If a group of electrons are drifted in an electric field (E_D) in a gas with attachment length λ, the number of free electrons decreases exponentially with an attenuation length of λ. Clearly, for satisfactory operation, a gas counter filling should exhibit an attachment length such that $\lambda/L >> 1$, where L is the active length of the detector. The attachment length is a very sensitive function of the molecular species and the electrostatic drift field and can vary rapidly over three orders of magnitude or more. It is consequently a strong determinant of what gases (and at what concentration) may be successfully employed in gas counters. This report reviews the fundamental processes involved, explores the effects of electron attachment on the performance of a GMSD and demonstrates a simple technique for characterising and minimising its adverse effects.

2. The effect of electron attachment on counter gain and energy resolution

The principal manifestations of electron attachment may be observed by studying the effects on the pulse height spectra of x-rays.

2.1 A simple model

The planar structure of the GMSD (with the drift electrode parallel to the detector plate containing the anodes) makes for a simple geometry. If we consider the uniform detection of N_0 monoenergetic x-rays (energy=E_x) in the drift gap of length L, then the effect of electron attachment is to convert the mean number of photoelectrons generated by the x-ray ($n_0 = E_x/w$, where w is the mean energy per ion pair in the gas) into a spectrum of pulse sizes (n):

$$\frac{dN}{dn} = \frac{N_0}{n}\frac{\lambda}{L} \qquad (1)$$

This is a "1/x" distribution which extends from n =$n_0$exp(-L/λ) to n_0. Integration of ndN/dn shows that the mean number of electrons detected is:

$$n_m = \frac{n_0 \lambda}{L}\left(1 - \exp\left(-\frac{L}{\lambda}\right)\right) \qquad (2)$$

The variance of pulse size distribution can be similarly evaluated to:

$$\sigma_n^2 = \frac{\lambda {n_0}^2}{L}\left[\frac{\left(1 - \exp(-2\frac{L}{\lambda})\right)}{2} - \frac{\lambda}{L}\left(1 - \exp(-\frac{L}{\lambda})\right)^2\right] \qquad (3)$$

Numerical examination of equation (3) shows that it can be approximated very closely by the simpler expression:

$$\sigma_n = 0.288 n_0\left(1 - \exp(-\frac{L}{\lambda})\right) \qquad (4)$$

The simple model thus shows that in the presence of electron attachment, the δ-function pulse height spectrum of a monoenergetic x-ray beam is shifted down in amplitude (equation (2)) and broadened (equation (4)). In the practical case the initial number of electrons (n_0) is dispersed in a normal distribution by the conversion process and the collected signal distribution (dN/dn) is further broadened by the avalanche process. In order to model these processes recourse must be had to Monte Carlo methods.

2.2 Monte Carlo Models

A typical x-ray line used to test gas counters is the K_α line of manganese at 5.9keV from a ^{55}Fe radioactive source. In an optimised GMSD this line gives a normal pulse height distribution of 14% FWHM (σ=5.9%). In the Monte Carlo model x-ray signals are generated randomly across the drift space and the detected electron signal attenuated by a chosen attachment length. These are then convolved with a normal distribution to incorporate the effects of photoelectron and avalanche statistics and simulate the detected pulse height spectra. The mathematical modelling (above) shows that the appropriate variable for quantifying the attachment is λ/L.

Figure 1 shows the simulated 5.9keV x-ray spectra as observed in a GMSD with values of λ/L ranging from 0.3 to 100. For λ/L<5 the spectra are extremely distorted and degraded with the functional form of equation (1) clearly visible for λ/L<1. However, for λ/L>10 there is a recognisable spectral line with the effects of attachment showing up as a small down-shift in the peak position and a slight broadening. Figure 2 summarises the behaviour of the mean and standard deviation of gaussian fits to the simulated distributions for λ/L>3. The means fit very well to the functional form of equation (2) (upper curve) and the standard deviation fits well to

the functional form of equation (4) added in quadrature with the photoelectron / avalanche width (lower curve).

3. A physical model of electron attachment

Gas counters are usually filled principally with (non-electronegative) noble gases with a quencher at the level of ≈10% and possible contamination at levels <1%. It is convenient therefore to consider a mixture of noble gas with just one electronegative component which represents a fraction *f* of the total gas content. (In the presence of multiple electronegative components, charge-exchange reactions between them can lead to considerably greater electron attachment than might be expected from any one component.) The concentration (molecules / unit volume) of the electronegative component may be written as fN_L where N_L is Loschmidt's number (2.688 x 10^{19} molecules / cc at NTP).

The electronegativity of a molecular species is quantified by the *attachment coefficient* (*h*) which defines the probability of the capture of an electron in any one scattering event. The cross-section for attachment is thus $h\sigma$ where σ is the total electron scattering cross-section of the electronegative component. *h* is a strong function of the average electron kinetic energy and hence of the detector drift field (E_D). Figure 3 shows the behaviour of *h* for air and chlorine in argon as a function of E_D.

The mean free path (MFP) for the attachment process can thus be written:

$$\Lambda = \frac{1}{fN_L h\sigma} \quad (5)$$

which in turn defines the mean lifetime of an electron before attachment occurs:

$$\tau = \frac{1}{fN_L h\sigma u} \quad (6)$$

where u is the average electron velocity ($u = \sqrt{(2\varepsilon/m)}$, where ε is the electron kinetic energy and m its mass).

Thus a population of free photoelectrons (n_0) decays with time according to:

$$n = n_0 \exp(-\frac{t}{\tau}) \qquad (7)$$

In order to achieve the amplification of all (or most) of the photoelectrons it is necessary to ensure that the collection time (T) in the detector is such that $\tau >> T$. Assuming 2% of air in argon (f=0.02) with h = 10^{-5}, and typical values for the electron energy and scattering cross-section, τ has a value of a few hundred nanoseconds. (See reference [2], which this analysis follows, for details.) This is comparable to the collection time in a typical gas counter so indicating that with this level of air present, the attachment will be severe and the pulse height spectrum degraded.

Equation (7) can be rewritten in terms of the distance drifted by the electrons in the detector using the relation $x=vt$ where v is the electron drift velocity:

$$n = n_0 \exp(-\frac{x}{v\tau}) \qquad (8)$$

From this it is clear that the attachment length is given by:

$$\lambda = v\tau = \frac{v}{fN_L h\sigma}\sqrt{\frac{m}{2\varepsilon}} \qquad (9)$$

Using a typical drift velocity (figure (4)) of a few cm/μs, the electron lifetime calculated for a 2% air contamination of a typical gas counter (a few hundred ns) translates into λ≈1cm.

Equation (8) folds in several variables which depend on the exact composition of the gas mixture and the mean electron kinetic energy (ε), which is in turn dependent on the drift field of the detector. Figure 3 shows how h depends on E_D for air and chlorine in argon. Figure 4 shows the dependence of v on E_D for some typical argon + methane gas mixtures. The electron energy ε increases smoothly with E_D for typical gas mixtures (e.g. argon + methane) according to a power law E_D^p, where p≈1.5 [3]. If we assume that the total scattering cross-section is not a strong function of the drift field, we can get an idea of the behaviour of λ as a function of E_D by evaluating the quantity $\frac{v}{hE^{0.75}}$ from the data available in figures 3 and 4. Figure 5 shows the results for air and chlorine in argon.

The first thing to note about figure 5 is that the ordinates for air and chlorine differ by two orders of magnitude. (If pure oxygen were considered instead of air, the ordinates would not be so dramatically different.) This confirms the common experience that halogens and halogenated gases are very poisonous in gas counters. Studies of attachment in RICH (ring imaging cherenkov) counters [4] showed that a contamination of 6ppm of the halocarbon C_5F_{12} in a gas mixture consisting of 75% methane + 25% ethane reduced λ from 10m to 0.3m. These results also confirm that the lower alkanes (used routinely as quenchers) on their own do not exhibit significant electron attachment.

The second interesting feature of figure 5 is the opposite sense of the dependence of λ on the drift field. The improvement of λ with E_D observed in most routine counter operation (in which the pollutant is air) may be reversed with different pollutan

4. Direct measurements of λ

The planar geometry of the GMSD makes it possible to measure the attachment length of electrons by directing a collimated x-ray beam into the drift space parallel to the electrodes at two different distances from the anode-cathode plane and measuring the relative positions of the x-ray peaks on a pulse height analyser (PHA). Taking the

logarithm of the ratio then gives λ in terms of the separation of the beams. This exercise was performed in a GMSD with 10μm anode strips, 90μm cathode strips and a pitch of 300μm filled with CO_2 gas. The drift gap was set at 13mm permitting a 10mm separation of the two beams.

Figure 6 shows a plot of the measured values of λ as a function of $V_d - V_c$. (V_d is the potential of the drift electrode and V_c that of the cathode with the anode held at earth.) In this case the variable x+c in the fit is equal to E_D/1.3 (V/cm) and it is seen that $\lambda \approx E_D^{1.39}$. The offset ($c$) on the x-axis arises because of the contribution of the bipolar electric field between the anode and cathode to the drift field. Electrostatic field modelling shows that the drift field is accurately constant from the drift electrode to within two pattern pitches of the plate. It can be represented by:

$$E_D = \frac{V_d - \beta V_c}{L} \qquad (10)$$

where the fraction β is determined by the ratio of the cathode width to the pitch and the drift depth (L). With the standard pitch of 300μm and L=10mm, β≈0.7.

The behaviour of λ with E_D in figure 6 compares reasonably well with the "air" curve in figure 5 confirming that air is the most likely contaminant of the gas. Exact agreement is not, of course, to be expected since the physical parameters in figure 5 do not refer to CO_2.

5. Indirect measurements of λ

The planar electric field configuration of the GMSD means that the electron drift and avalanche gain processes are almost (but not quite) separated. Thus, as shown by equation (10) the drift field is mostly determined by V_d with a lesser contribution from V_c. Similarly it is found [5] that the gain is determined by the notional potential V' (= $V_c + \alpha V_d$) where $\alpha \approx 0.007$ for the counters used in these tests. Over the limited range of gain controlled by V_d the gain can be accurately represented by an exponential function:

$$M = \exp\{A + B(V_c + \alpha V_d)\} \qquad (11)$$

For fixed V_c, this implies that:

$$M = \exp(a + bV_d) \qquad (13)$$

If we consider the detection of x-rays in the presence of electron attachment during the drift, the gain (or pulse height) measured at a given V_d will be (equation (2):

$$M(V_d) = \frac{\lambda}{L}\left(1 - \exp\left(-\frac{L}{\lambda}\right)\right)\exp(a + bV_d) \qquad (14)$$

where λ is also a function of V_d as discussed above. Figure 7 shows the behaviour of M as a function of V_d with two different gas mixtures as measured with 5.9keV x-

rays. In the case of argon + 5% isobutane there is no significant attachment so that the gain formula (13) fits to the data over the whole available range of V_d. In the case of a mixture with 75% isobutane the behaviour of M is clearly strongly affected by the attachment term in equation (14) and only at high drift fields does the gain curve asymptote to equation (13) as λ/L becomes >> 1.

This behaviour is reproduced in most gas mixtures and the basic gain $M_0(V_d)$ (zero attachment) is estimated by fitting the high V_d points of the gain curve (figure 7) to equation (13). The attachment term of equation (14) is now obtained by evaluating $M/M_0(V_d)$. The problem is now to solve the equation

$$\frac{\lambda}{L}\left(1-\exp\left(-\frac{L}{\lambda}\right)\right)=\frac{M}{M_0} \qquad (15)$$

for λ. This is not possible in an explicit form. However, as shown in Appendix 1 it is possible to derive an accurate power series expansion (figure 8):

$$L/\lambda = 2(1-M/M_0) + 0.72618(1-M/M_0)^2 + 3.3435(1-M/M_0)^3 \qquad (16)$$

Gain versus V_d plots such as those instanced in figure 7 were measured for gas mixtures ranging from 5% to 100% isobutane in argon using 5.9keV x-rays in the standard GMSD (10μm anodes, 90μm cathodes, 300μm pitch with 10mm drift gap). The gain was fitted at the highest V_d points and $M/M_0(V_d)$ evaluated over the range of V_d. Equation (16) was now used to evaluate λ/L from M/M_0.

Figure 9 shows the curves thus derived for λ/L as a function of V_d-0.7V_c (since L = 1cm , E_D(V/cm) is numerically equal to V_d-0.7V_c). The good linear ln-ln fits show that the relation $\lambda \approx E_D^p$ holds for all gas mixtures but that the exponent p varies strongly with the percentage of isobutane. Figure 10 shows this graphically. The conclusion from the graphs is that while λ declines dramatically with increase in the isobutane concentration, the accompanying rapid increase of the exponent of the drift field means that increasing the drift potential can restore the situation quite effectively.

Figure 11 shows the behaviour of λ/L at a fixed drift field (500 V/cm) as a function of the isobutane concentration. Experience with isobutane has suggested that there is an electronegative pollutant in it which can (on occasion) make a bottle of the gas unusable. In this case one might expect to see a curve behaving as “1/f” (equation (9)) However, apart from noting that it is approximately linear from 5% to 80% concentration, it is impossible to draw any conclusions as to the determining processes since, as equation (9) shows, λ depends on the drift velocity and the electron temperature which vary strongly with the gas composition.

It will be noted that in figure 9 the derived values of λ/L become increasingly noisy as λ/L rises. This follows from the fact that $\lambda/L \approx 1/P(1-M/M_0)$ where P is the polynomial function specified in equation (16). The stochastic noise inherent in the pulse height (gain) measurement is rapidly amplified by this transformation as $M/M_0 \rightarrow 1$ and sets a limit to the maximum value of λ/L which may be measured with significant precision. In addition, there is a systematic error induced by the procedure

of fitting the gain to the points with the highest V_d. This inevitably causes the value of λ/L to be overestimated in this region since we have forced M/M_0 to be unity. These limitations mean that λ/L can only be estimated with reasonable precision for regions in which $1-M/M_0 > \delta M$ (the stochastic error in M) and V_d lies below the gain normalisation region.

6. The effect of electron attachment on X-ray spectra

It is clear from the mathematical model and the simulations (equations (2), (4) and figure 2) that the presence of significant electron attachment causes a pulse height deficit and a broadening of the x-ray pulse height peaks. While the latter causes a loss of energy resolution, the former can induce non-linearity in the energy response.

6.1 X-ray energy resolution

Experimentally, the energy resolution of an x-ray line in a GMSD is routinely measured as the relative full width at half maximum (FWHM) in percent. Converting the SD as defined in equation (2) to this parameter gives a contribution from the electron attachment effects of:

$$F_{att} = 236 * 0.288\left(1-\exp(-\frac{L}{\lambda})\right)$$

i.e.

$$F_{att} = 68\left(1-\exp(-\frac{L}{\lambda})\right)$$

Adding the intrinsic (photoelectron and avalanche statistics) FWHM (F_I) in quadrature gives an estimate for the x-ray line:

$$F = \sqrt{F_I^2 + 68^2\left(1-\exp(-\frac{L}{\lambda})\right)^2} \qquad (17)$$

Figure 9 shows that λ is a rapid function of the drift field ($E_D = (V_d - 0.7V_c)/L$). One would expect equation (17) to describe the behaviour of F as a function of V_d using the simple power law fits used in figure (9). That is, we set $\lambda = k(V_d-0.7V_c)^p$.

Figure 12 shows the experimental measurements of the FWHM of 5.9keV x-rays as a function of the drift potential for a range of gas compositions (argon + isobutane, 5%-100%) in the standard GMSD (10μm anodes, 90μm cathodes, 300μm pitch with 10mm drift gap). Equation (17) is fitted with F_I (a in the fits), *L/k* (*b* in the fits) and *p* (*c* in the fits) as free parameters. Good fits can be obtained but it is obvious that while the values of *p* (*c*) are in the same general range as the exponents derived from the gain data (figure 10), the agreement is poor.

The reason for this is quite clear from the experimental data, which shows that while electron attachment clearly has a strong effect on the energy resolution at low drift fields, there are other processes which become dominant in particular circumstances.

For example, on inspection of the curve for argon + 10% isobutane (figure 12) it is clear that there is an independent process which causes the FWHM to rise significantly as V_d increases. This is discussed in detail in reference [6]. Another independent process is revealed in the behaviour of F_I (a) in the fitted data. F_I is seen to minimise at 13.9% at an isobutane fraction of 10%, rising on either side. Thus while the behaviour of λ with V_d is seen to have a very significant effect on the FWHM, this measurement is not suitable for quantifying λ because of the interaction of other, independent processes.

The general conclusion to be drawn from figures 12 and 9 is that when λ/L drops below ≈10 (i.e for isobutane fractions >50% over most of the range of V_d) then the energy resolution for 5.9keV x-rays is significantly degraded by electron attachment effects. This is in good agreement with the simulation results presented in figures 1 and 2. Raising V_d continuously to reduce λ is not an option because other processes cause the FWHM to increase. There is in general an optimum V_d for the FWHM and this optimum V_d value rises as λ decreases and the optimum FWHM also increases.

6.2 X-ray energy non-linearity

In the model of section 2, the x-rays are assumed to convert uniformly in the drift space (e.g. via a side window). If the x-rays enter through the drift electrode (as is often the case) the x-ray beam attenuates as it traverses the drift space with an attenuation length Λ. As Λ changes with energy the spatial distribution of conversion electron packets changes and the mean fraction of the ideal pulse height detected (n_m/n_0) changes leading to non-linearity in the x-ray energy scale. To estimate this effect one must repeat the analysis of section 2 with the x-rays distributed along the drift axis according to $dN/dx = N_0/\Lambda \exp((L-x)/\Lambda)$ instead of $dN/dx = N_0/L$. For convenience we measure x from the plate back towards the drift electrode.

With this modification equation (1) for the pulse height distribution now becomes:

$$\frac{dN}{dn} = \frac{\lambda N_0 n_0^{\gamma} \exp(-L/\Lambda)}{\Lambda n^{1+\gamma}} \qquad (18)$$

where $\gamma = \lambda/\Lambda$. Equation (18) can be used to derive the mean of the pulse height distribution in the usual way. The result is:

$$n_m = \frac{n_0 \lambda}{(\Lambda - \lambda)} \exp(-L/\Lambda) \frac{(1 - \exp(-L(1/\lambda - 1/\Lambda)))}{(1 - \exp(-L/\Lambda))} \qquad (19)$$

where Λ is, of course, a function of the x-ray energy.

Figure 13 shows a plot of n_m/n_0 as a function of the x-ray energy for a drift space of 20mm filled with argon at 1 bar. Clearly, values of $\lambda/L < 10$ can result in distortions of the energy calibration by the order of a few percent. While this may seem negligible compared with the energy resolution of 14% (FWHM) for 5.9keV x-rays, the centroid of the peak can be measured to a precision of $14/\sqrt{N}$% where N is the number of counts in the peak. Since routinely, $N > 10^4$ a non-linearity of a few percent will be a noticeable problem in the x-ray energy calibration.

The effects of attachment on the energy linearity can be minimised by avoiding gas absorption edges in the working energy range and Λ can be minimised by diluting the absorbing gas, all be it at the expense of detection efficiency.

7. The effect of electron attachment on auger electron spectra

When the GMSD is used for the detection of auger electrons from a sample which forms the drift cathode, as in EXAFS applications [7], the gas composition is usually arranged so that the maximum range of the most energetic electrons (R) is ≈1mm. The pulse heights reaching the amplifying plane now lie in the range $n_0\exp(-L/\lambda) < n < n_0$, and the variation in the mean (n_m) is $\approx n_0R/\lambda$. Considering the case of a strongly electronegative gas with $\lambda/L = 1$ in a detector with L = 10mm, it follows that the pulse heights will be reduced by a factor of exp(-1) (0.368) with a spread (FWHM) of ≈0.1/1 (10%) in the values. This broadening of the pulse height spectrum will scarcely be noticeable when convolved with the intrinsic pulse height resolution (15% - 30%) in the electron energy range of interest (1.5keV – 6keV). Thus we can conclude that, provided sufficient gas gain (and electronic signal to noise performance) can be obtained to compensate for the loss of signal, auger electron energy spectra may be successfully detected in gas atmospheres with $\lambda \approx$1cm, corresponding (for example) to ≈ 2% of air in an argon mixture.

8. Monitoring Gas Purity

The analysis of sections 5 and 6 show that a simple series of measurements of the pulse height analyser peak position (gain) and FWHM of an x-ray line such as the 5.9keV of Mn (^{55}Fe radioactive source) can be used to detect electronegative contaminants at the levels relevant to detector operation. In other words, with this set of measurements the detector can be its own gas monitor.

Dimethyl ether (DME) is the quencher of choice when gas counters must be used in very intense beams since it resists the polymerisation processes which cause the degradation of such quenchers as ethane and isobutane. However, for a long gas lifetime the DME must be free of contaminants such as oxygen. The combination of DME and oxygen appears to be particularly electronegative, so the x-ray pulse height spectra are effective as a monitor of the gas purity. A GMSD x-ray detector was constructed using only ceramic and stainless steel components and connected up to stainless steel gas mixing system which supplied a mixture of argon + 29% DME. The strip pattern was the standard one described above and fabricated in gold on S8900 glass with a 9mm gap to a beryllium drift cathode. Gas flow was initiated and plots of the gain and FWHM versus V_d made at intervals over the following 48 days.

Figure 14 shows the plots of the relative gain (normalised at high V_d as described in section 5) versus V_d throughout this period, and figure 15 shows the corresponding plots of the FWHM versus V_d. Both show systematic changes over the purge period. The FWHM, while strongly time-dependent at the lowest V_d, gives slightly ambiguous results, whereas the relative gain shows clear changes with time. Applying the transformation of equation (16) to this data yields the plots of λ/L shown in

figure 16. Here the characteristic behaviour $\lambda \approx kE_D^p$ is observed (i.e. approximately a straight line on a ln-ln plot) with $2 < p < 3$. It is not clear from the data whether the apparent saturation of λ/L at V_d >1500V is real or just a result of the stochastic measurement noise beginning to dominate.

The gradual clean-up of the counter and gas system over the 48 day purge period is shown clearly in figure 17, where L/λ at V_d = -1200V and V_d = -1600V are plotted as a function of time. Looking at equation (9) we note that if we hypothesise a single electronegative pollutant (e.g. oxygen), then with V_d constant and all other gas conditions held constant, the fraction of pollutant present (*f* in equation (9)) should be proportional to L/λ. In general the concentration of a pollutant will decay exponentially under a steady purge. As figure 17 shows, the V_d = -1600V data gives a reasonable fit to a decaying exponential with a lifetime of 22.8 days. The V_d =-1200V data gives a similar fit but the data is considerably noisier.

Acknowledgements

It is a pleasure to acknowledge the contributions of my colleagues, J.F. Connolly, R. Stephenson, D.M. Duxbury and J.A. Mir to the design, construction and operation of the equipment from which the results described above were obtained.

References

1. Oed, Nucl. Instr. & Meth. **A263** (1988) 351-359

2. F. Sauli, Principles of operation of multiwire proportional and drift chambers, CERN/77-09/1977

3. V. Palladino and B. Sadoulet, Nucl. Instr. and Meth. **128** (1975) 323

4. D. Fraissard, S. Haider, H. Hofmann, H. Jansen, W Klempt, R. Lalloz, E. Rosso and D. Soria, Nucl. Instr. and Meth. **A252** (1986) 524

5. J.E. Bateman, J.F. Connolly, G.E. Derbyshire, D.M. Duxbury, J. Lipp, J.A. Mir, R. Stephenson, J.E. Simmons and E.J. Spill, Studies of the gain properties of Gas Microstrip Detectors relevant to their application as X-ray detectors, Rutherford Appleton Laboratory Report, RAL-TR-1999-057, (http://www-dienst.rl.ac.uk/library/1999/tr/raltr-1999057.pdf) Presented at the International Workshop on Micro-Pattern Gas Detectors, Orsay, France, 28-30 June 1999.

6. Energy resolution in X-ray detecting gas microstrip detectors, J.E. Bateman, J.F. Connolly, G.E. Derbyshire, D.M. Duxbury, J.A. Mir, E.J. Spill and R. Stephenson, Rutherford Appleton Laboratory Report RAL-TR-2000-022, (http://www-dienst.rl.ac.uk/library/1999/tr/raltr-2000022.pdf)

7. T. Rayment, S.L.M. Schroeder, G.D. Moggridge, J.E. Bateman, G.E. Derbyshire and R. Stephenson, Rev. Sci. Instr. **71** (2000) 3640

8. S.C. Brown, Basic Data of Plasma Physics, MIT Press, Cambridge, Mass., 1959

9. H.W. Fulbright, Ionisation Chambers in Nuclear Physics, in Encyclopaedia of Physics, (Ed. S. Flugge) Springer Verlag, Berlin, 1958, p1

Appendix 1

The problem is to find a power series expansion for the solution of λ/L as a function of M/M_0 in the equation:

$$\frac{\lambda}{L}\left(1-\exp\left(-\frac{L}{\lambda}\right)\right)=\frac{M}{M_0} \qquad \text{(A1)}$$

First we change to the variables $y = L/\lambda$ and $x = M/M_0$ when equation (A1) becomes:

$$x = \{1 - \exp(-y)\}/\, y \qquad \text{(A2)}$$

Now consider the case of low attachment, i.e. $x << 1$. Expanding the exponential function in equation (A2) and keeping only the first order term we get:

$$x \approx 1 - y/2 \qquad \text{(A3)}$$

Rearranging we get:

$$y \approx 2(1-x) \qquad \text{(A4)}$$

Figure 8 shows the approximation (A4) compared with the target function (A1). As expected the approximation is only valid for small values of y ($L/\lambda < 0.2$). However, the form of the target function encourages us to generalise the first approximation (A4) by including higher order terms of a power series in (1-x). i.e.

$$y = 2(1-x) + a(1-x)^2 + b(1-x)^3 \qquad \text{(A5)}$$

where a and b are constants obtained from least squares fitting process. Figure 8 shows that the values a = 0.72618 and b = 3.3435 give an excellent approximation ($r^2 = 0.99988$). We thus have the good approximation:

$$L/\lambda = 2(1-M/M_0) + 0.72618(1-M/M_0)^2 + 3.3435(1-M/M_0)^3 \qquad \text{(A6)}$$

valid over the range commonly encountered in the experimental data: $0.4 < M/M_0 < 1$.

Figure Captions

1. Simulated pulse height spectra for a 5.9keV x-ray line detected in a GMSD with varying degrees of electron attachment in the gas. λ is the electron attachment length and L is the depth of the drift region.

2. The peak position and the relative standard deviation (σ_{rel}) of the simulated x-ray pulse height spectra are compared with the mathematical models (equations (2) and (4)) as a function of the parameter λ/L.

3. The attachment coefficient for electrons in air and an argon-chlorine mixture as a function of the drift electric field [8]. Note the factor of 1000 difference in the vertical scales.

4. The drift velocity of electrons [9] in various mixtures of argon-methane as a function of the drift electric field.

5. Plots of the parameter $v/(hE_D^{0.75})$ calculated using the data of figures 3 and 4 (v is the drift velocity, h the attachment coefficient and E_D the drift field), showing how λ may be expected to vary with drift field for air and chlorine contamination of argon-methane gas mixtures. Note the hundred-fold difference in the vertical scale.

6. The electron attachment length as a function of drift field measured experimentally in pure CO_2 in a GMSD. The term c in the fit takes account of the contribution of the cathode potential to the drift field (equation (10)).

7. The gain of a GMSD as measured from a 5.9keV x-ray line peak pulse height as a function of the drift potential in argon gas mixtures with different fractions of isobutane. The fits show the expected exponential gain curve when the attachment becomes negligible (i.e. $\lambda/L >> 1$). In this detector L = 10mm.

8. A plot of the approximate solutions obtained in appendix 1 for the explicit expression of L/λ in terms of the apparent relative gain (M/M_0) derived from plots such as those of figure 7.

9. The attachment length as a function of drift field (E_D) derived from gain versus V_d plots for various argon-isobutane gas mixtures. The drift gap (L) is 10mm.

10. The exponent (p) of the fits of the form $\lambda/L = kE_D^p$ to the data of figure 9, plotted as a function of the isobutane fraction in the gas mixture.

11. The attachment length (λ/L) at a constant drift field of 500V/cm as a function of the fraction of isobutane in the gas mixture (from the data of figure 9).

12. The experimentally measured FWHMs of the 5.9keV x-ray line are plotted as a function of the drift potential for the range of argon-isobutane gas mixtures. The fitted curves are of the form of equation (17).

13. The non-linearity of the x-ray energy response induced by electron attachment is shown as the fraction of the true pulse height ($\lambda >> L$) measured at a given x-ray energy in a gas with different attachment lengths (equation (19)).

14. The measured relative gain (M/M_0) of the 5.9keV x-ray line, plotted as a function of the drift potential for a high integrity GMSD design as a function of the purge time, showing the slow clean-up of the system.

15. The measured FWHM of the 5.9keV x-ray line plotted against the drift potential during the purge period of the high integrity GMSD design.

16. The electron attachment length calculated from the data of figure 14 as the GMSD and gas system are purged.

17. The inverse electron attachment length (L = 9mm) at V_d = -1200V and V_d = -1600V for the high integrity GMSD plotted against the purge time. This is proportional to the fraction of electronegative impurity present.

FIGURE 1

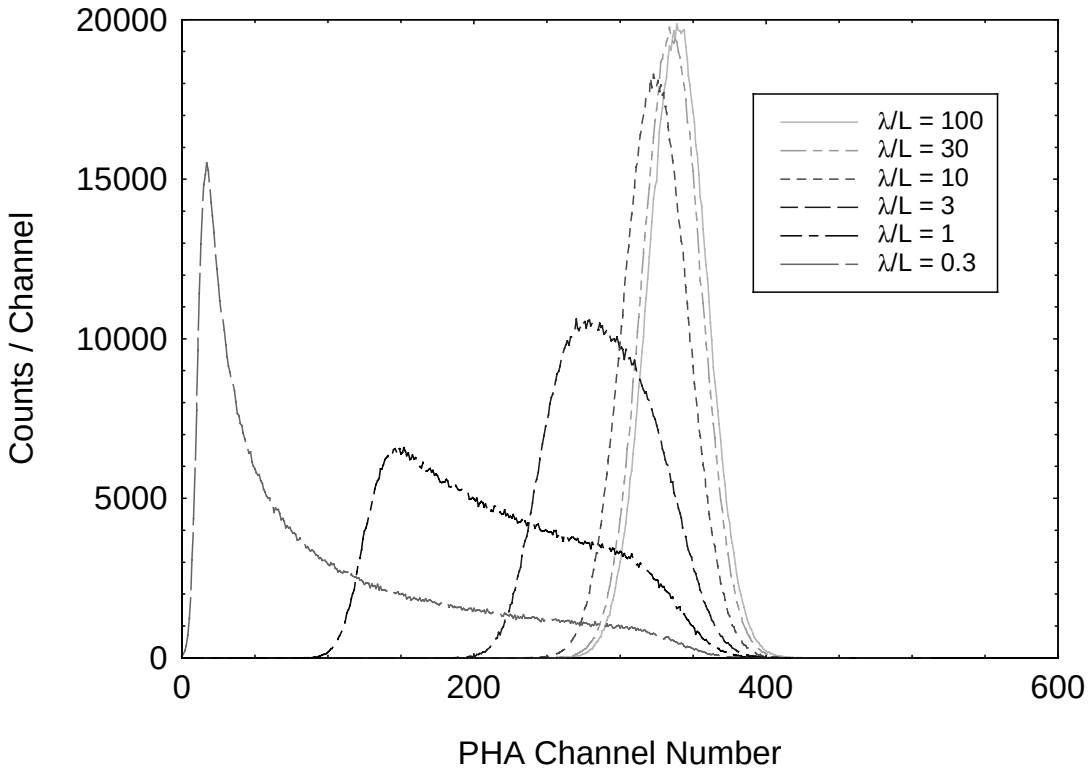

FIGURE 2

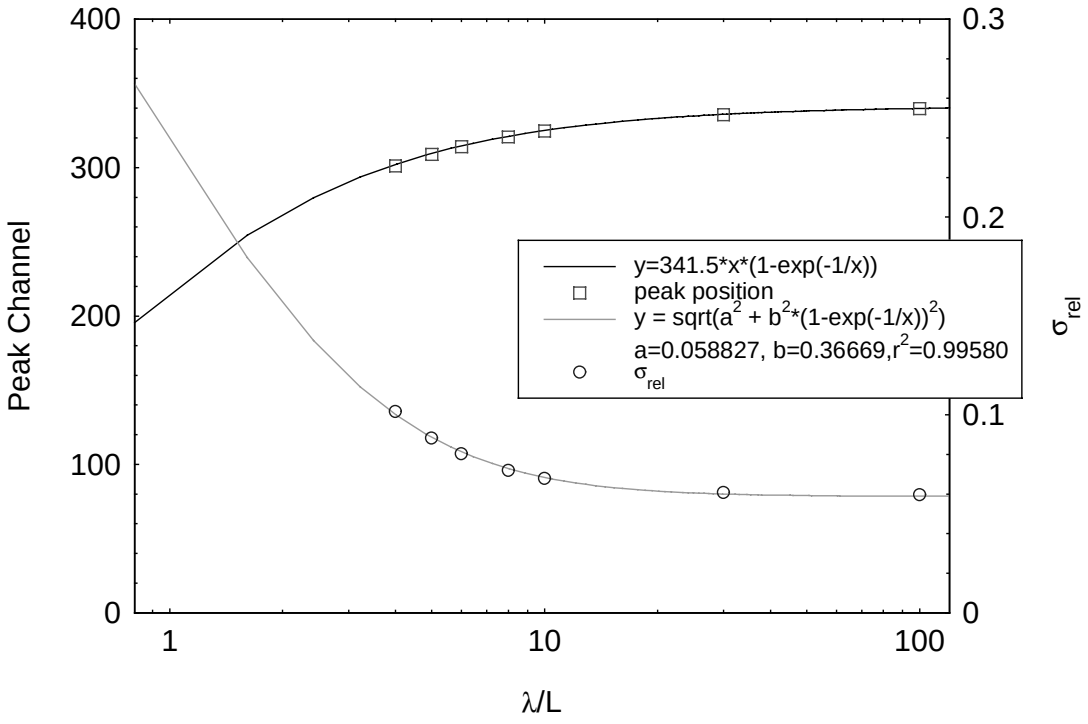

FIGURE 3

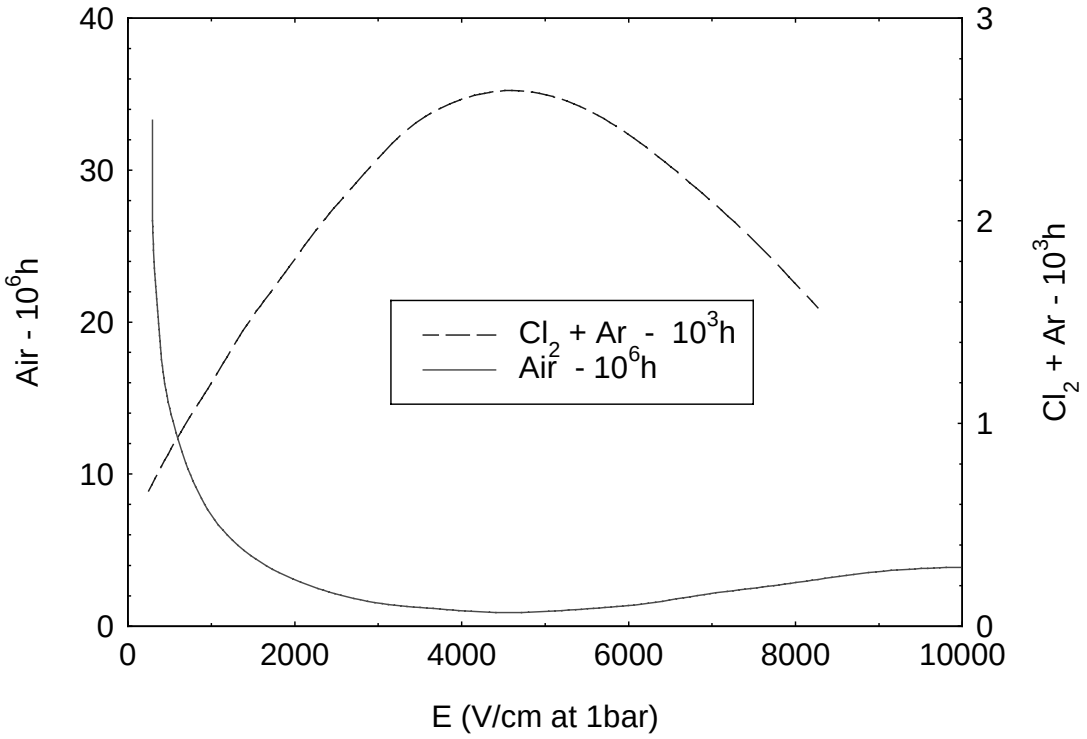

FIGURE 4

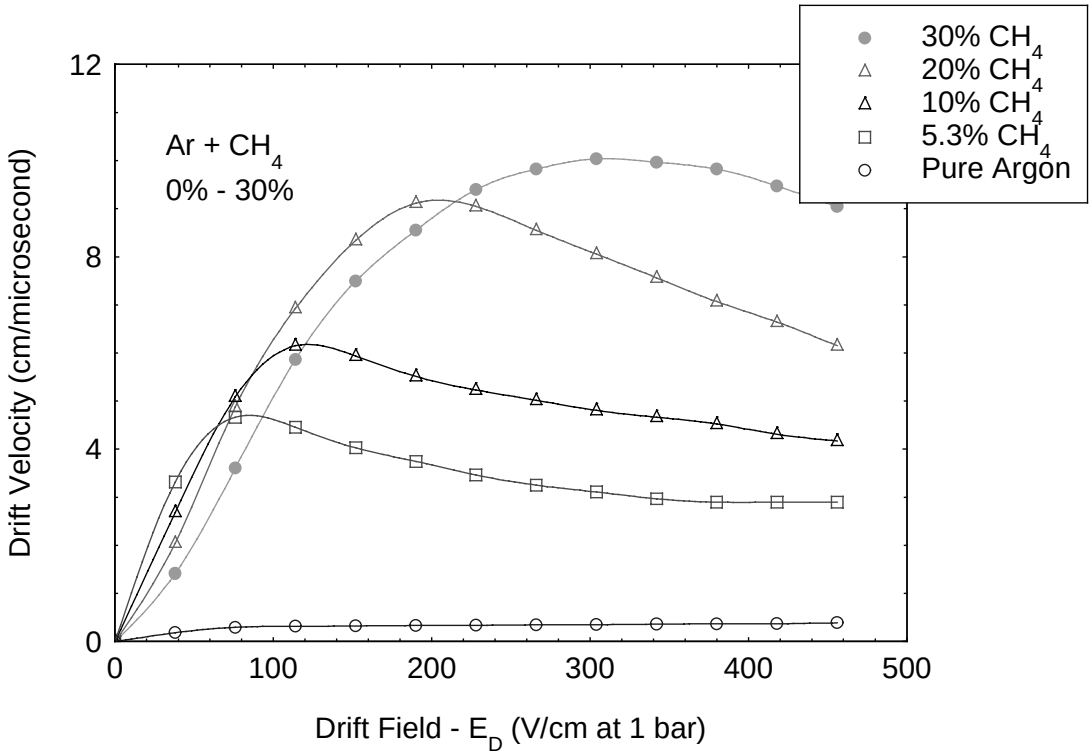

FIGURE 5

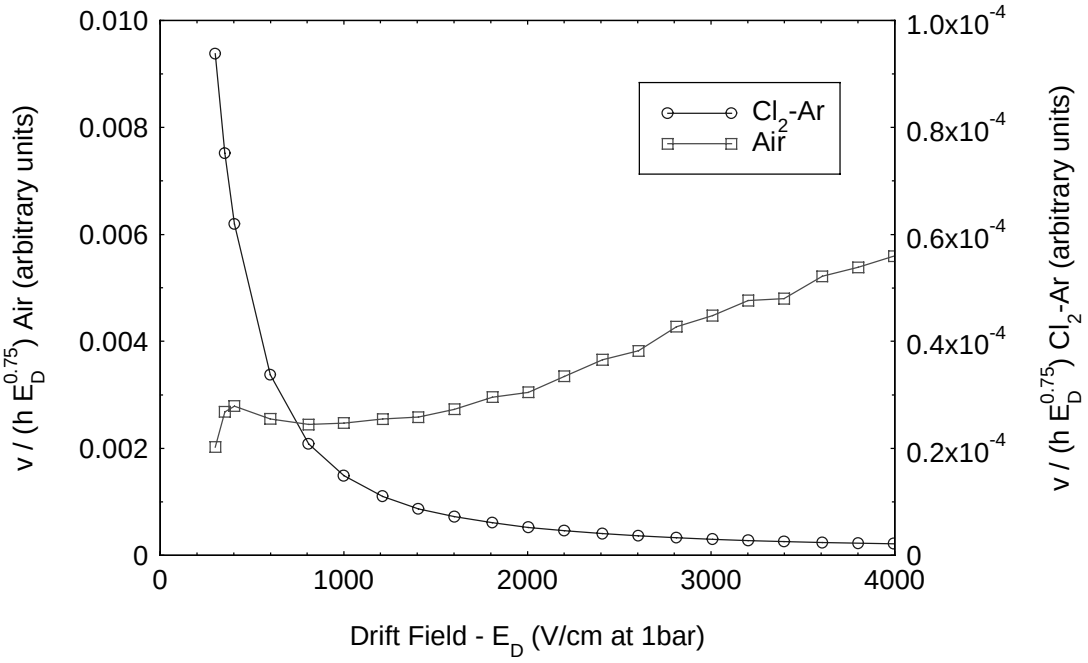

FIGURE 6

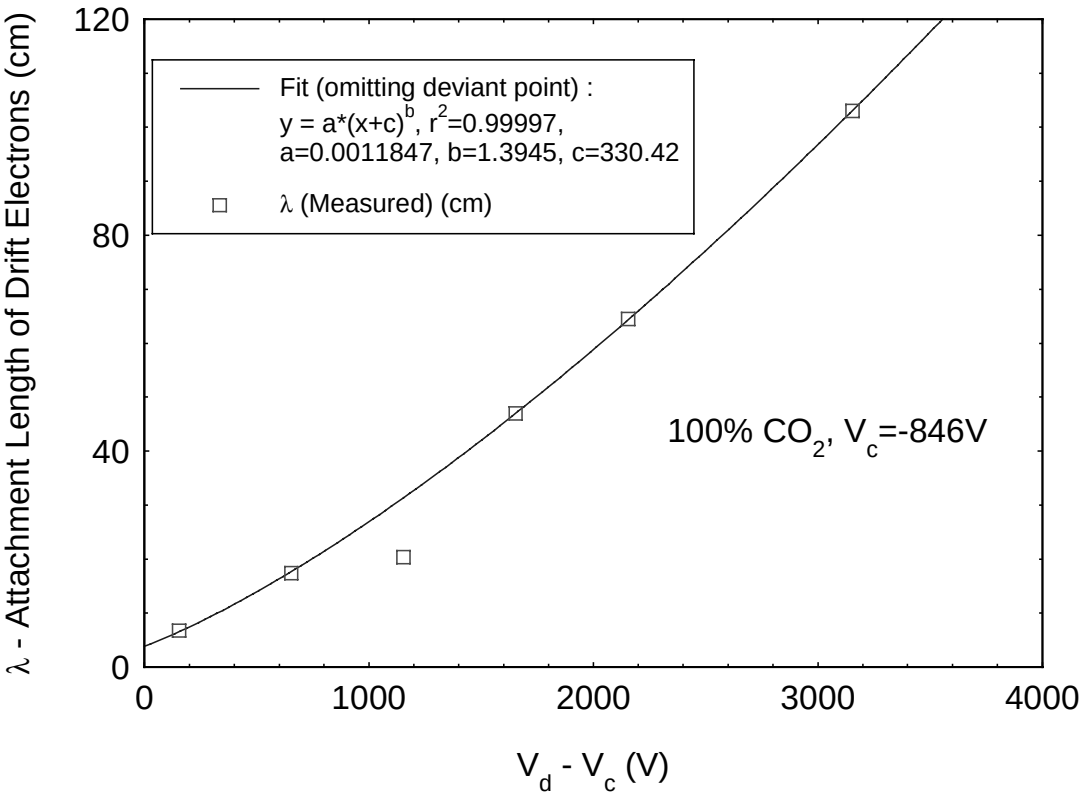

FIGURE 7

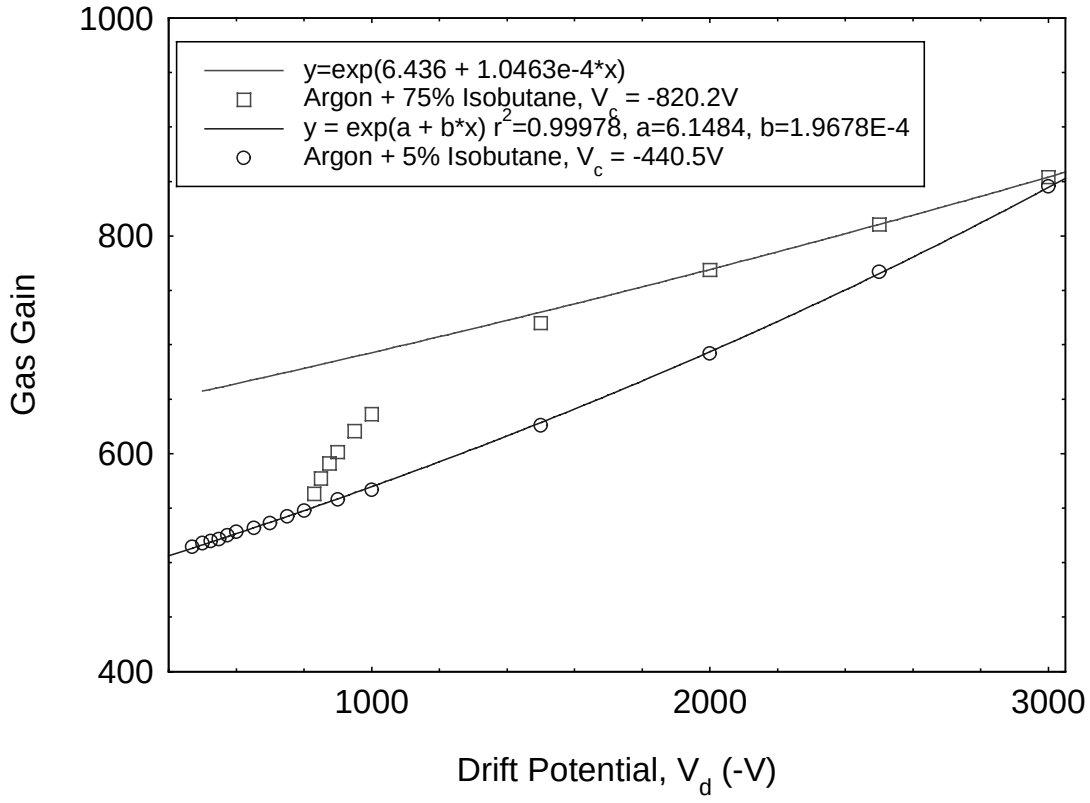

FIGURE 8

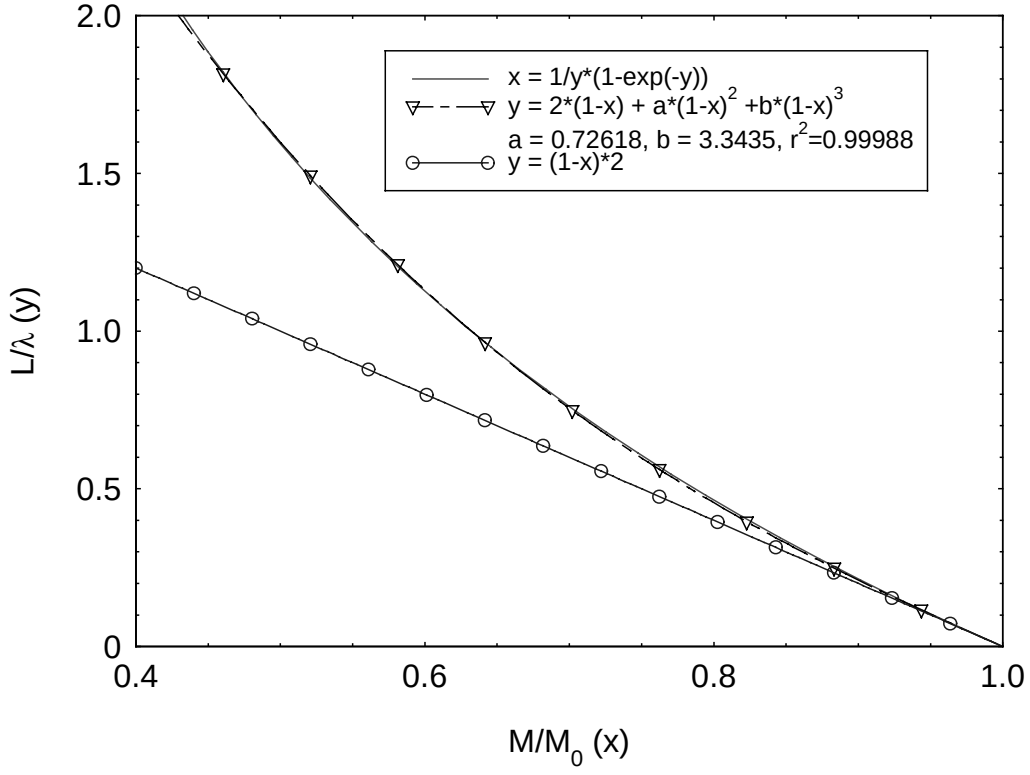

FIGURE 9

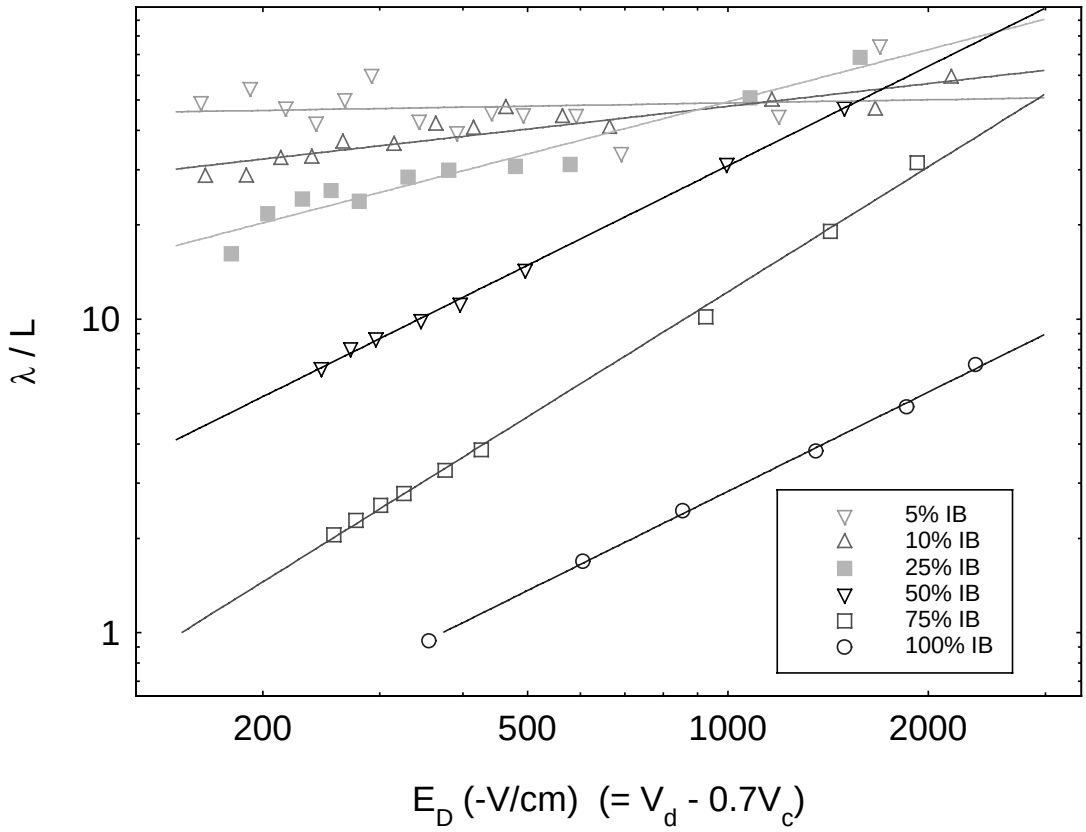

FIGURE 10

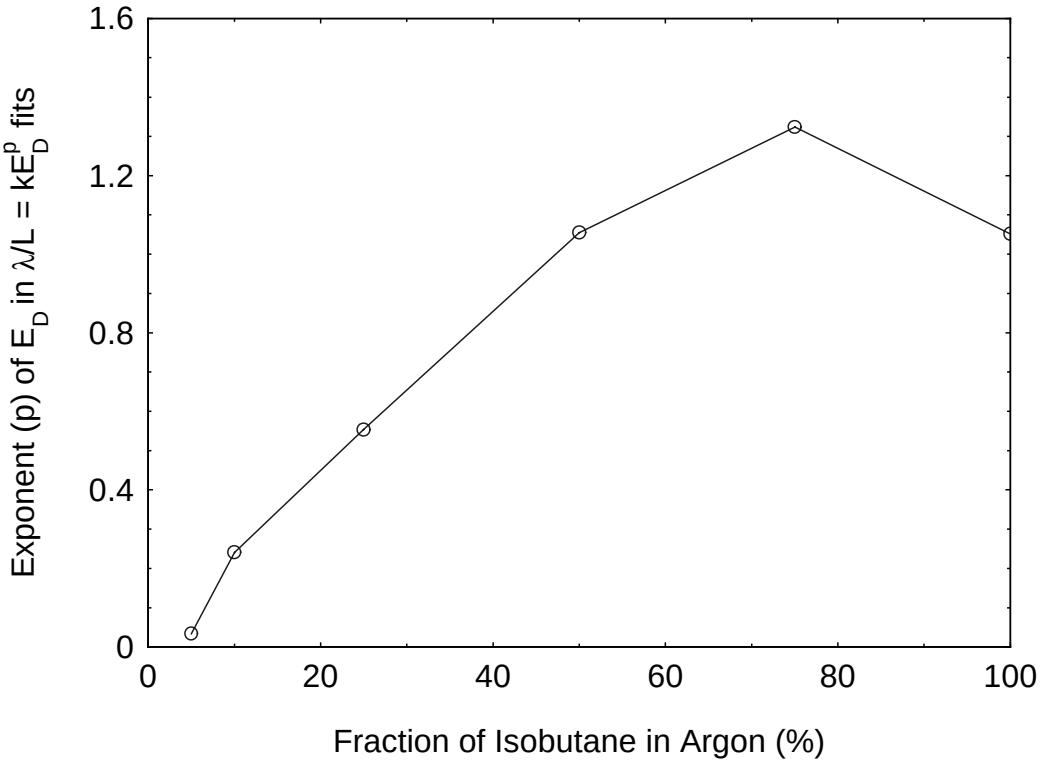

FIGURE 11

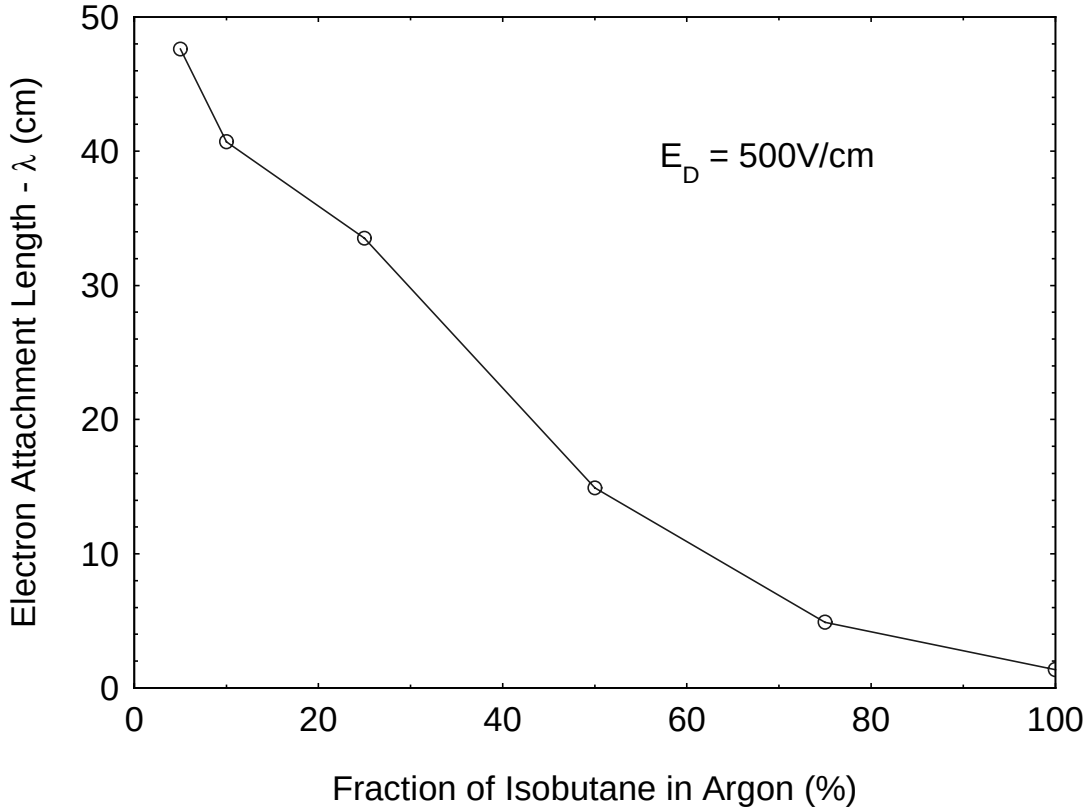

FIGURE 12

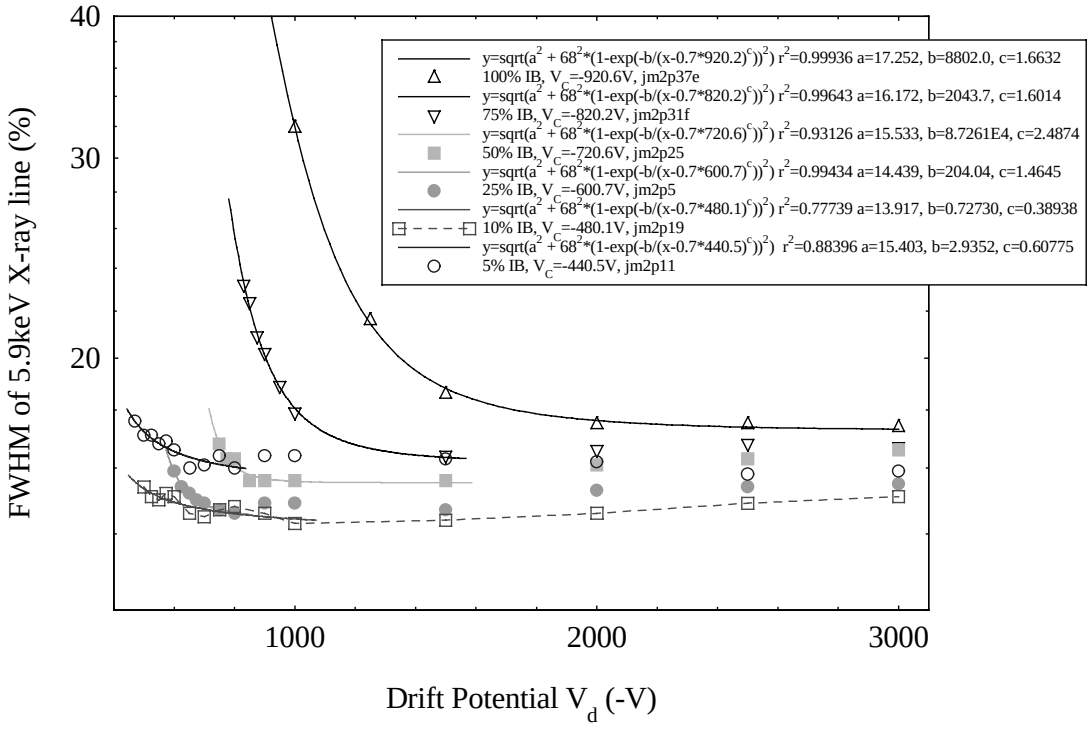

FIGURE 13

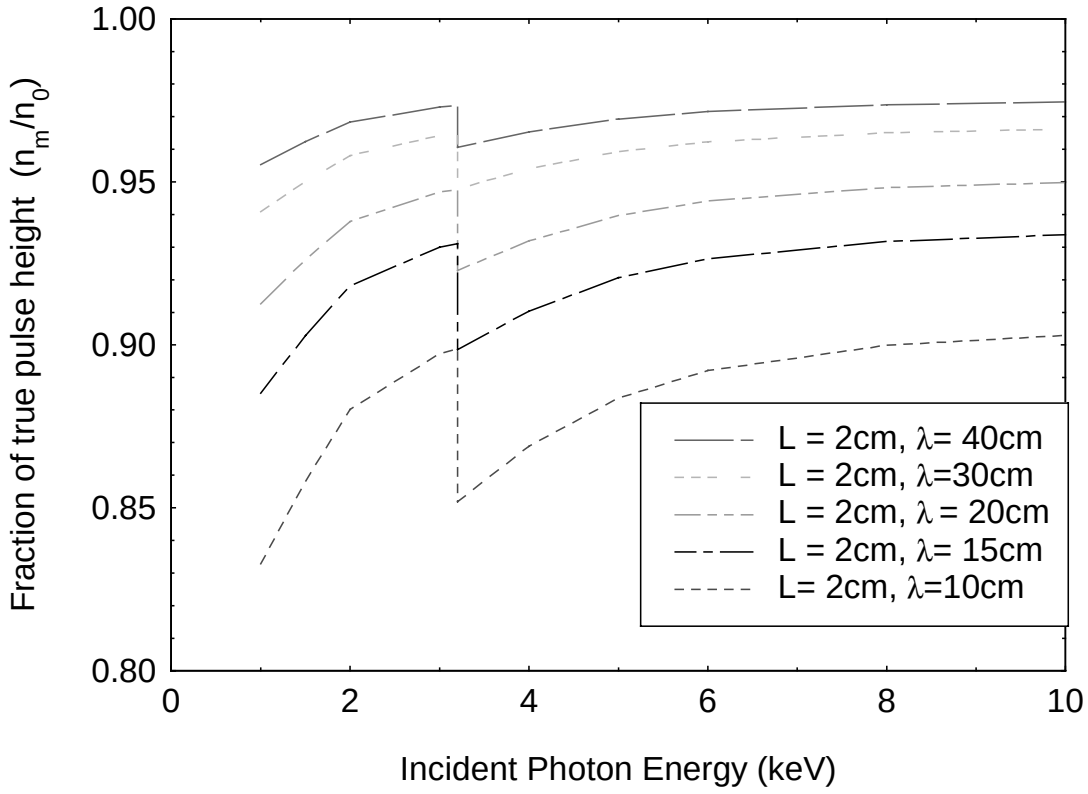

FIGURE 14

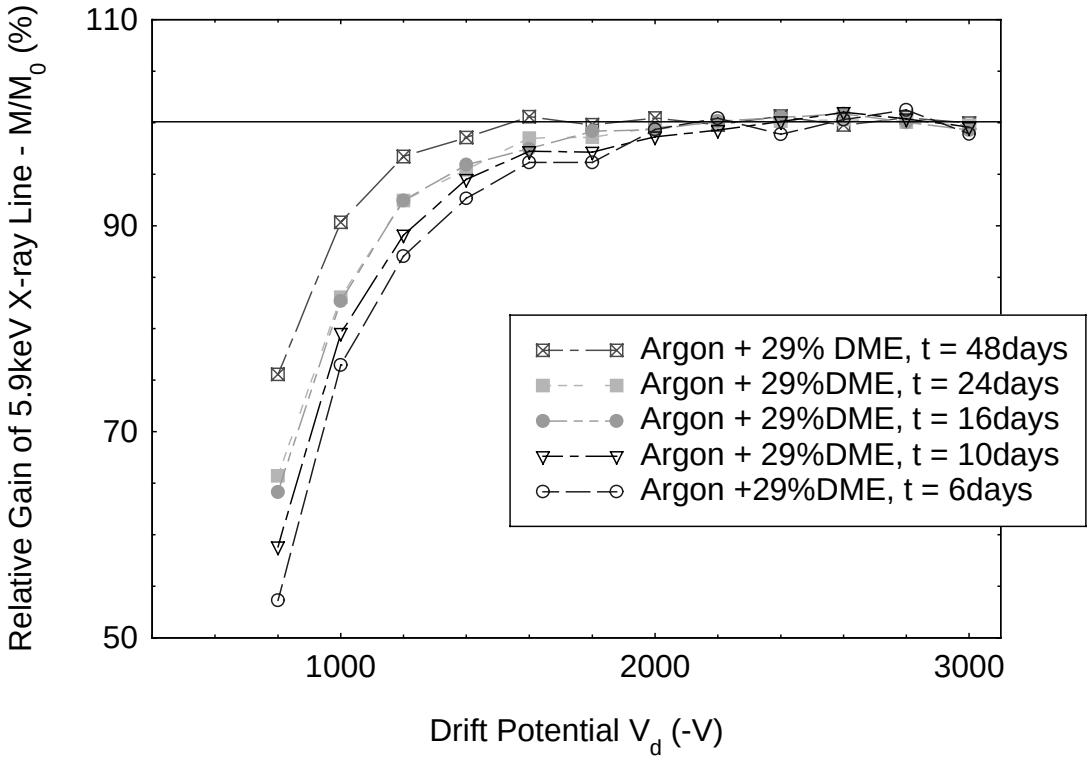

FIGURE 15

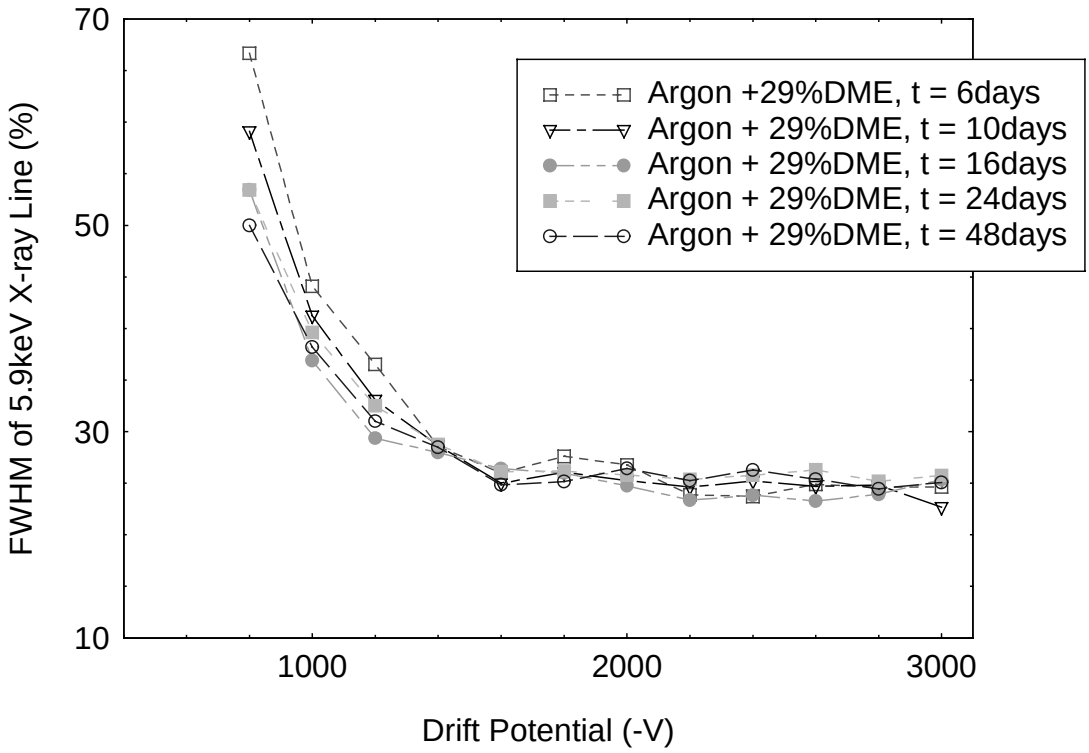

FIGURE 16

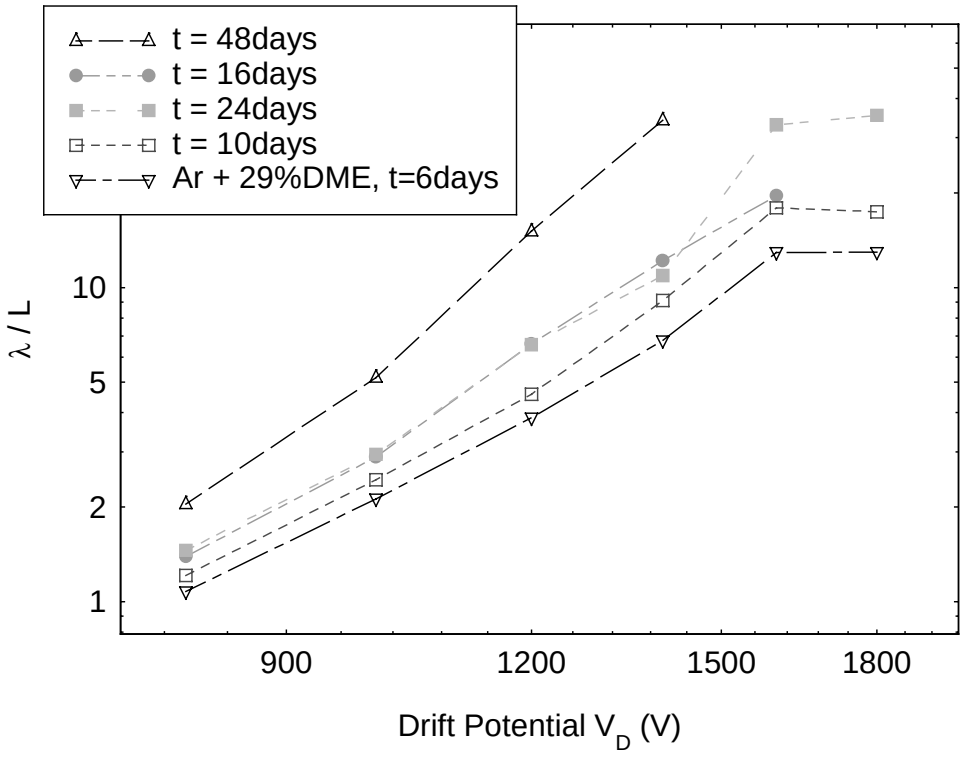

FIGURE 17

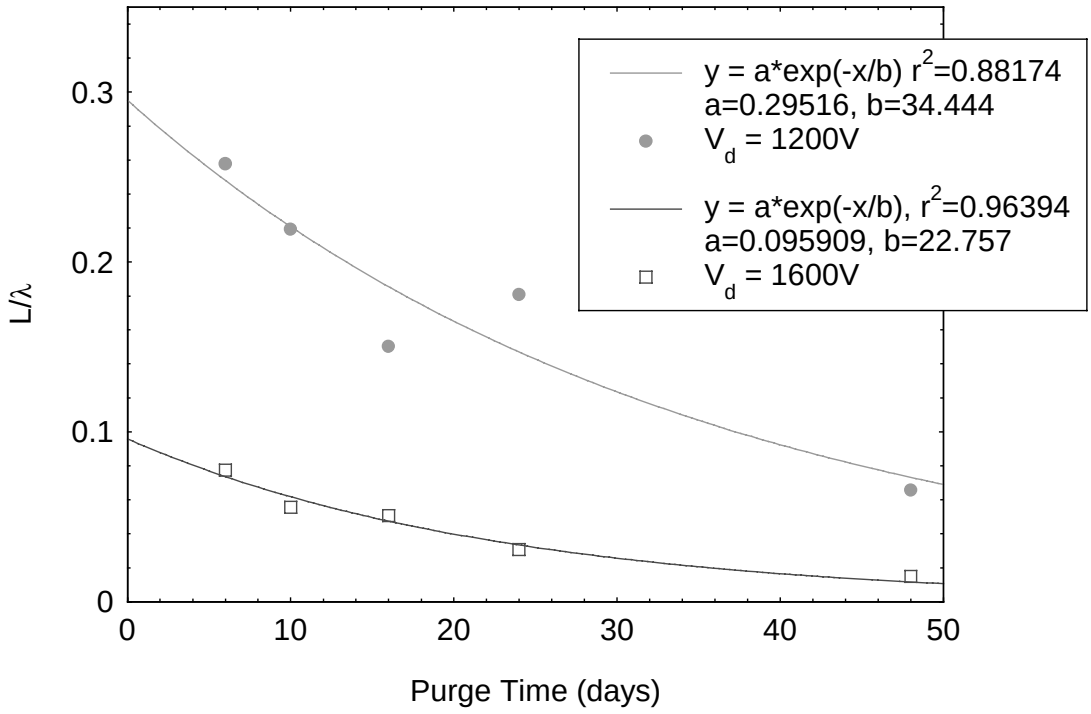
y = a*exp(-x/b) r2=0.88174
a=0.29516, b=34.444
Vd = 1200V
y = a*exp(-x/b), r2=0.96394
a=0.095909, b=22.757
Vd = 1600V
L/λ
0
0.1
0.2
0.3
0
10
20
30
40
50
Purge Time (days)